Dynamic keyhole: A novel method to improve MR images in the presence of respiratory motion for real-time MRI

Danny Lee, Sean Pollock, Brendan Whelan, Paul Keall and Taeho Kim

Radiation Physics Laboratory, Sydney Medical School, University of Sydney, Sydney, Australia

Corresponding Author: Taeho Kim, Ph.D.

Radiation Physics Laboratory, Sydney Medical School, University of Sydney

Room 475, Blackburn Building D06

The University of Sydney

NSW Australia 2006

(phone): 61 2 9351 3385 (fax): 61 2 9351 4018

e-mail: taeho4kim@gmail.com

ABSTRACT

Purpose: In this work, we present a novel MRI reconstruction method to improve the quality of MR images in the presence of respiratory motion for real-time thoracic image-guided radiotherapy.

Methods: This new reconstruction method is called Dynamic Keyhole and utilizes a library of previously acquired, peripheral k-space datasets from the same (or similar) respiratory state in conjunction with central k-space datasets acquired in real-time. Internal or external respiratory signals are utilized to sort, match, and combine the two separate peripheral and central k-space datasets with respect to respiratory displacement, thereby reducing acquisition time and improving image quality without respiratory-related artifacts. In this study, the dynamic keyhole, conventional keyhole, and zero-filling methods were compared to full k-space acquisition (ground truth) for sixty coronal datasets acquired from 15 healthy human subjects.

Results: For the same image-quality difference from the ground-truth image, the dynamic keyhole method reused 79% of the prior peripheral phase-encoding lines, while the conventional keyhole reused 73% and zero-filling 63% (p-value < 0.0001), corresponding to faster acquisition speed of dynamic keyhole for real-time imaging applications.

Conclusions: This study demonstrates that the dynamic keyhole method is a promising technique for clinical applications such as image-guided radiotherapy requiring real-time MR monitoring of the thoracic region. Based

on the results from this study, the dynamic keyhole method could increase the temporal resolution by a factor of five compared with full k-space methods.

Keywords: real-time imaging; thoracic imaging; motion artifacts; respiratory motion; radiotherapy guidance

I. INTRODUCTION

There are a number of medical applications in interventional radiology and cancer radiotherapy that require real-time patient images to continuously monitor the region of interest for therapeutic guidance.[1-4] Magnetic resonance imaging (MRI) is an ideal candidate for these applications; it has excellent soft-tissue contrast, does not expose subjects to ionizing radiation,[5] and is capable of both anatomical and functional imaging. Recently, radiotherapy systems integrated with MRI have been proposed by Kolling (2013),[6] Viewray Inc. (2011),[7] Raaymakers (2009),[8] and Fallone (2009).[9]

In order to be utilized for real-time imaging,[10-12] a technique offering both fast and quasi-continuous image acquisition and reconstruction is required for MR image guidance. However, thoracic imaging in conventional MRI often suffers from motion artifacts[13] and long scan times, which are not suitable for image-guided therapeutic procedures. Hence, there is a need for methods that can reduce scan times without inducing respiratory-related artifacts in the images of the thoracic region.

One method to speed up MR image acquisition is to exploit the basic structure of the raw datasets (digitized MRI signals) in k-space (Fourier transform of the MR image). Central (low-frequency) k-space datasets contain the majority of the image information, while peripheral (high-frequency) k-space datasets are associated with fine image details, such as edge definition and image sharpness. In applications requiring real-time imaging, undersampling k-space datasets directly corresponds to a reduction in imaging time.[14]

Conventionally, the unmeasured datasets are simply filled with zeros in a technique called zero-filling,[15] but this results in image blurring, low image resolution and contrast. An improvement to zero-filling is the conventional keyhole technique.[14, 16, 17] In this case, the missing data are filled with a previously measured single peripheral k-space dataset. The conventional keyhole method allows continuous motion to be monitored with an acceptable level of image quality in cases where motion is negligible. But, in cases in which the range of motion is large, there will be a mismatch between the previously obtained peripheral dataset and the central k-space datasets. This mismatch can result in significant image artifacts, particularly in large field of view (FOV) imaging due to longer acquisition times.

Other undersampling techniques to reduce both acquisition time and motion sensitivity are circular,[18] radial[19], and spiral[20] undersampling. In these approaches, unmeasured points can still cause artifacts due to zero-filling, interpolation, and oversampling in duplicated data.[21, 22] The large FOV in thoracic imaging limits these undersampling schemes due to the out-of-field object size exceeding the diameter of FOV.[18] The speed of acquisition can be accelerated using compressed sensing[23] in some applications. However, this requires computationally-intensive iterative reconstruction[24], leading to a delay between image acquisition and reconstruction which is a barrier to real-time applications. This limits the applicability of these undersampling techniques in the thoracic region, in which respiration can cause significant organ motion and a large field of view is often required.[25-28] As yet, an effective technique for real-time imaging in these regions has not been proposed.

In this study, we introduced a new reconstruction method called Dynamic Keyhole, which utilizes a library of previously acquired prior peripheral k-space datasets for the same (or similar) respiratory state in conjunction with the central k-space datasets. In this method, real-time internal or external respiratory signals were utilized to sort, match, and combine the two separate peripheral and central k-space datasets with respect to respiratory displacement. In addition, we demonstrated that the dynamic keyhole method can reduce MR image acquisition time, as well as improve image quality in the presence of respiratory motion in the thoracic region. Image reconstruction performance was compared using sixty MRI datasets from fifteen healthy human subjects. The dynamic keyhole method was compared with the conventional methods: zero-filling and conventional keyhole.

II. METHODS

The following sections describe the processes of the dynamic keyhole method, its implementation, and a retrospective simulation to test its efficiency compared to the zero-filling and conventional keyhole methods.

II.A. Dynamic Keyhole Method

The dynamic keyhole method is an extension of the conventional keyhole method.[14] Instead of using a single prior peripheral k-space dataset, the dynamic keyhole method uses a library of prior peripheral k-space datasets, each corresponding to a different respiratory displacement. Hence, rather than matching a prior peripheral k-space dataset of a particular respiratory displacement to every central k-space dataset across a range of respiratory displacements, the dynamic keyhole method selects and closely matches peripheral k-space datasets from the library, with the central k-space datasets taken in real time and combined with the prior k-space

datasets by respiratory displacement matching. A comparison between the dynamic keyhole method and the conventional keyhole method is shown in Figure 1.

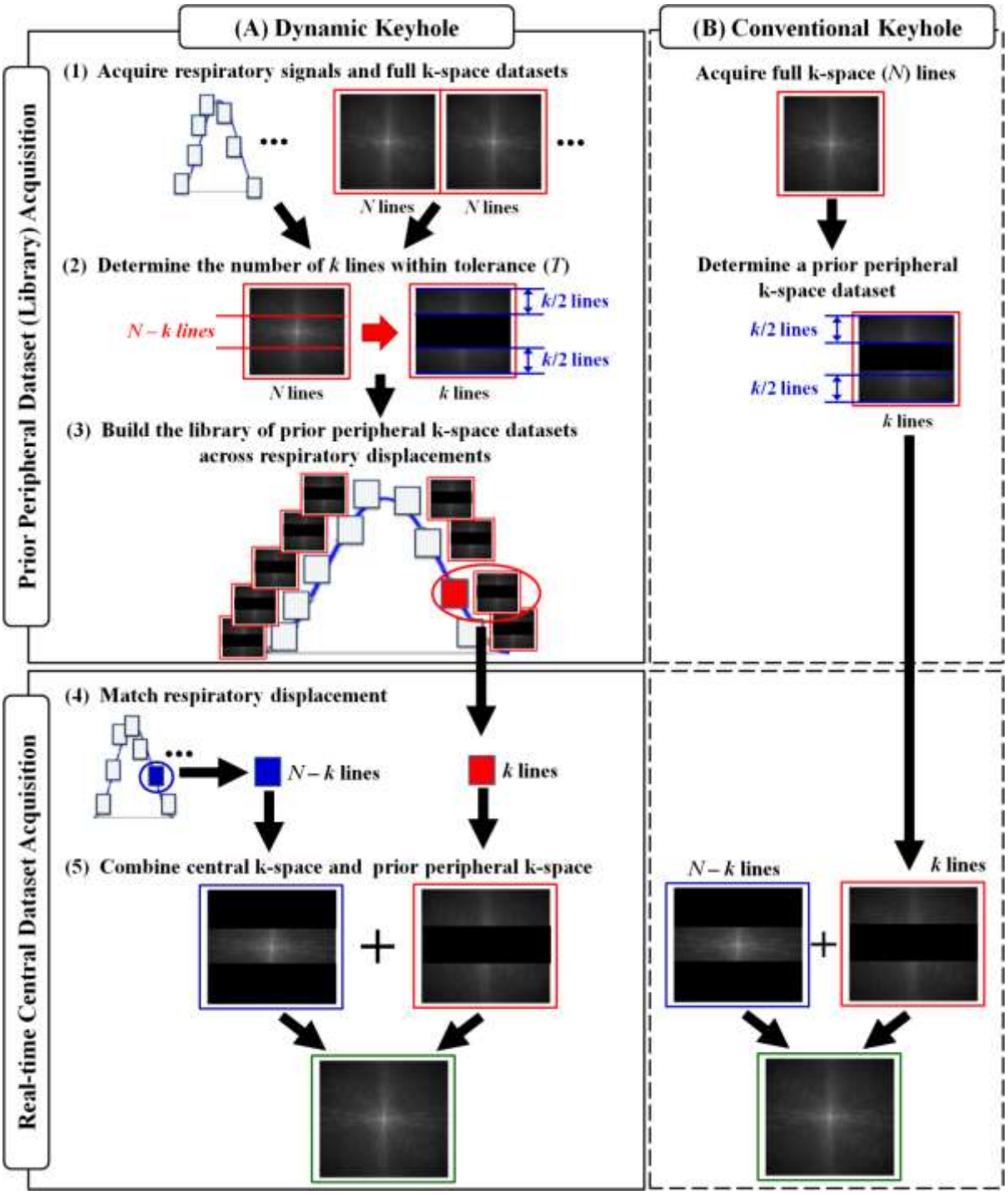

Figure 1. The dynamic keyhole method (A) compared to the conventional keyhole method (B). The conventional keyhole method uses a single prior peripheral k-space dataset while the dynamic keyhole method uses a library of multiple prior peripheral k-space datasets across a range of respiratory displacements.

The dynamic keyhole method is composed of two processes: (1) Acquiring a library of prior peripheral k-space datasets; (2) Acquiring real-time central k-space datasets. Respiratory signals are utilized to improve a match of the library of prior peripheral k-space datasets with central k-space datasets, resulting in fast MR imaging by undersampling k-space, while minimizing respiratory-related artifacts. Each of these steps is explained in detail below.

II.B. Prior peripheral k-space dataset (library) acquisition

In this retrospective study using existing datasets, five respiratory cycles of about twenty seconds were initially used, based on clinical MRI respiratory-gating practice,[29] to build the library of prior peripheral k-space datasets, using the following steps:

1. In Figure 1(1), respiratory signals were continuously acquired. Full k-space datasets were synchronized with the respiratory signal, beginning at peak inhalation and ending after five respiratory cycles. The synchronized respiratory signals and full k-space datasets can be expressed as $Lib(d_{n,}\, N)$, where d is respiratory displacement, n is the n^{th} full k-space dataset and N is the number of full k-space phase encoding lines (N = 256).
2. At the end of the five respiratory cycles, $Lib(d_{n,}\, N)$ was sorted with respect to unique respiratory displacements $Lib'(d_{m,}\, N)$, where m is the m^{th} position of the respiratory displacement from the peak inhalation with a millimeter bin width, and reconstructed using a 2D Fourier Transform, $I(Lib'(d_{m,}\, N))$. A tolerance T, which represents a fraction δ of average image intensity $\overline{I(Lib'(d_{m,}\, N))}$ determined on a pixel-by-pixel basis, was chosen and used as a measure of image quality. The tolerance T can be expressed as

$$Tolerance\ (T) = \overline{I(Lib'(d_{m,}\, N))} \times \delta \qquad (1)$$

In this study, we used δ=0.1 (10%) of $\overline{I(Lib(d_{m,}\, N))}$ for the tolerance, which corresponds to the typical image quality achievable by conventional keyhole method. Then, the number of prior peripheral k-space phase-encoding lines, k, was determined within T in Figure 1(2).

3. In Figure 1(3), the library of prior peripheral k-space datasets, $Lib'(d_{m,}\, k)$ acquired at the same respiratory displacements from d_1 to d_m, was reconstructed using $256 - k$ lines ($k = 1, 2, \ldots, 255$). Each reconstructed image was compared with the image reconstructed using 256 lines, and k was increased until the difference between the two images exceeded T. If there were more than two k-space

datasets with the same respiratory displacement, the process was repeated and the average value of k was used to form the library.

For the zero-filling and conventional keyhole reconstructions, the k lines of N with zeros (zero-filling) or a single dataset taken in the mid-exhalation phase (conventional keyhole) was determined using a similar process as described in the three steps above. The k lines of zeros (zero-filling) or the k lines of a single dataset (conventional keyhole) were increased until the difference of the two images exceeded T.

II.C. Real-time central k-space dataset acquisition

The real-time central k-space dataset acquisition began after the library acquisition. In this instance, the size of the central k-space datasets ($N - k$ lines) was determined through matching respiratory displacement between a present respiratory signal and the matched dataset of the library, shown in Figure 1(4). Then, the ($N - k$ lines) of central k-space dataset were combined with the k lines of the matched dataset in Figure 1(5).

II.D. Testing the dynamic keyhole method

In order to investigate the efficacy of the dynamic keyhole method compared to the zero-filling and conventional keyhole methods, the three methods were implemented in Matlab version 7.13 (The MathWorks, Natick, USA) and tested retrospectively using respiratory and MR image datasets acquired in a previous study.[30] Sixty MRI datasets with associated respiratory motion datasets were acquired from fifteen healthy human subjects in the supine position using a 3T GE MR scanner (GE Healthcare, Waukesha, USA). Each subject had a total of four MRI scans over two separate imaging sessions. Each dataset consisted of 512 images in the 2D coronal plane acquired approximately every 200 ms using fast gradient recalled echo (fGRE) pulse sequence with a field of view (FOV) of 480 × 384 mm^2 and a 96 × 96 matrix size per frame across more than twenty respiratory cycles. Each MR image was interpolated to a 256 × 256 matrix by the MR scanner. Internal respiratory signals (5Hz) were obtained from each MR image at the peak of the right diaphragm of the dome of the liver. The Real-time Position Management (RPM) system (Varian Medical Systems, Palo Alto, USA) was used to monitor the subjects' abdominal respiratory motion to obtain external respiratory signals (30Hz). Overall, for these datasets, the correlation of internal and external signals was found to be very high in a previous study, an average Pearson's R-value of 0.96.[31] The 30 Hz external signal was downsampled to the temporal resolution of 5 Hz for (1) the use of respiratory displacements at the closest acquisition time between

respiratory signals and full k-space datasets in Figure 1(3), and (2) the use of the sixty datasets acquired at 5 Hz temporal resolution during the acquisition of central k-space datasets in Figure 1(4).

The dynamic keyhole method was compared with the zero-filling and conventional keyhole methods in two ways: firstly, by evaluating the acquisition speed for the same image quality and secondly, by evaluating the image quality at the same acquisition speed[14]. For the first comparison, the acquisition speeds of the methods were quantified by using the number of *k* lines reused by each method to achieve the same image quality. For the second comparison, the quality of the images reconstructed from the same number of *k* lines was compared with the quality of the original ground-truth image reconstructed from the full k-space datasets by using the differences in image intensity.

The impact of the use of internal or external respiratory signals was also investigated. The number of *k* lines required to achieve the same image quality was quantified for both respiratory signals for each of the three methods. Quantitative statistical comparison of the performance was determined using the mean, standard deviation, and paired Student's t-test (Excel 2010, Microsoft, Redmond, USA).

III. RESULTS

The correlation between faster image acquisition and better image quality for the zero-filling, conventional keyhole, and dynamic keyhole methods is shown in Figure 2.

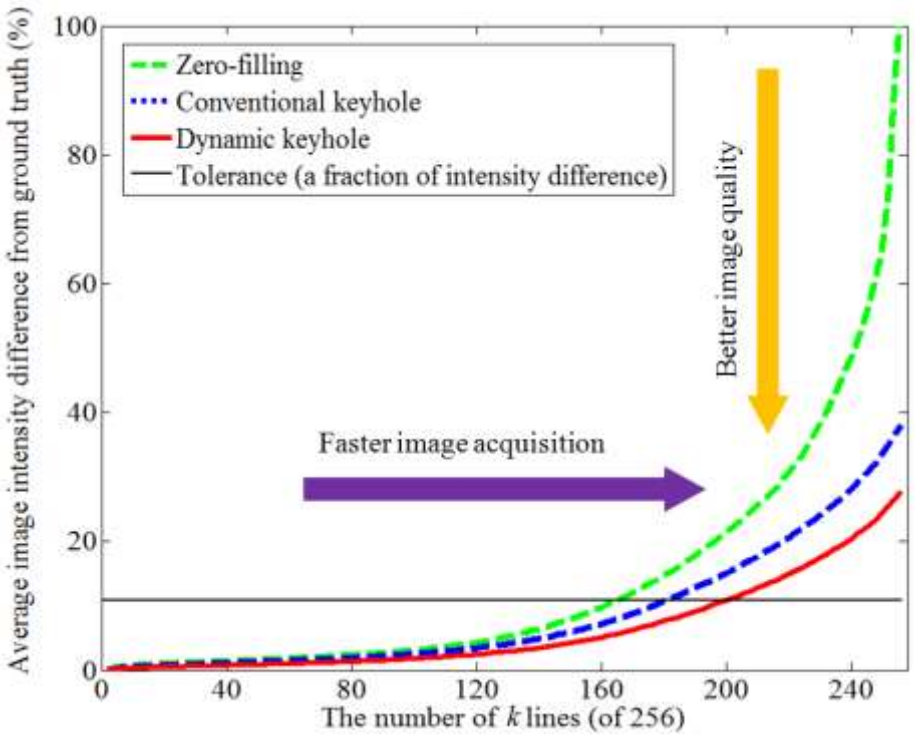

Figure 2. The relationship between faster image acquisition (horizontal arrow) and better image quality (vertical arrow) for each of the three methods tested.

The intersections of each of the curves with the tolerance, which is 10% of average image intensity (thin, horizontal black line), indicate the number of *k* lines that were reused for each method. The image intensity difference increased when the number of *k* lines was increased in all three methods, but was smallest in the dynamic keyhole method. This showed that the dynamic keyhole method can reuse more *k* lines for the same image quality, resulting in faster image acquisition.

Figure 3 shows reconstructed images using the different number of *k* lines required to produce the same image quality compared to original ground truth image.

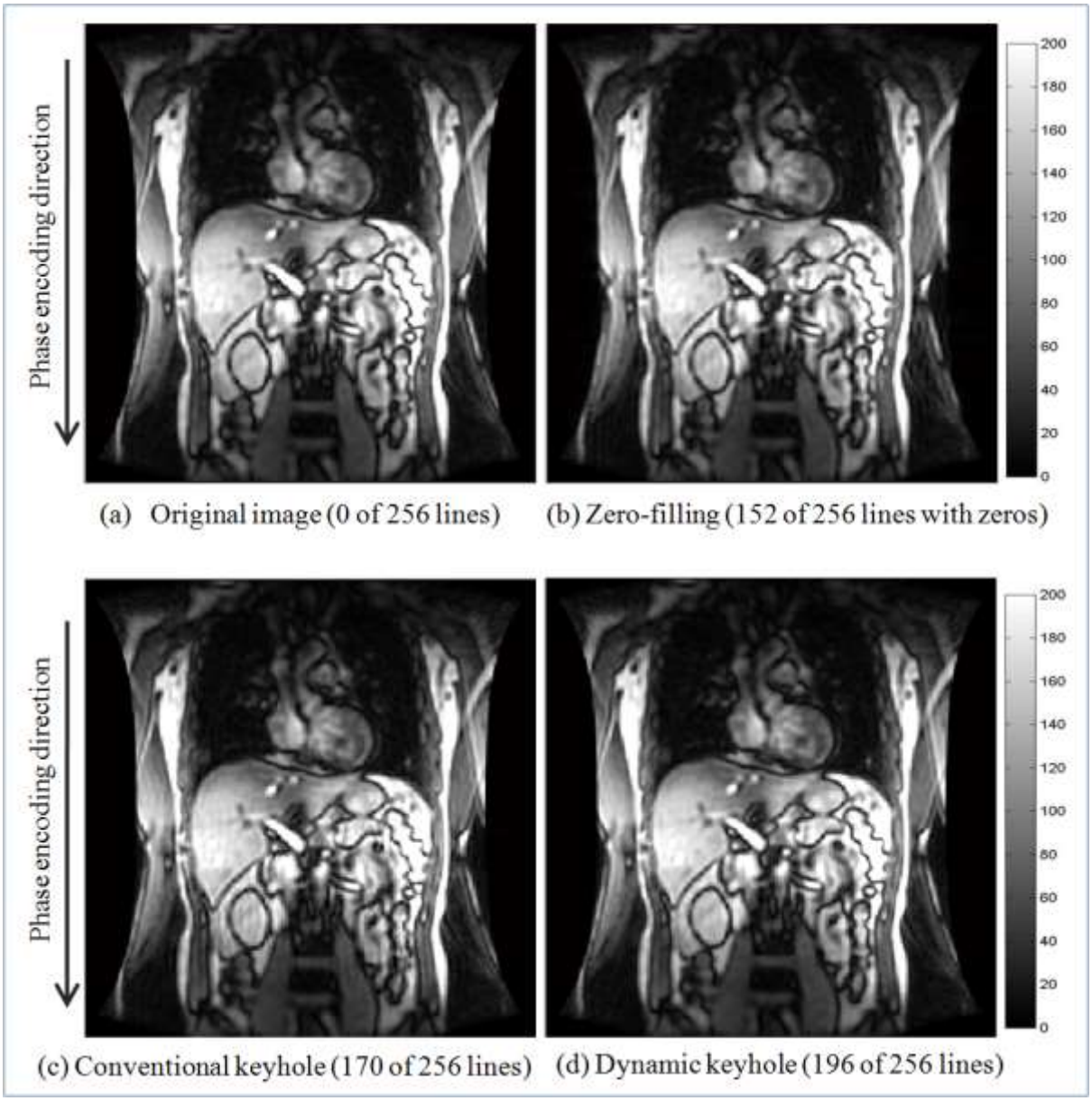

Figure 3. Reconstructed images using the different number of *k* lines required to produce the same image quality compared to original ground truth image: (a) original image (*k* = 0 lines), (b) zero-filling reconstructed image (*k* = 152 lines with zeros), (c) conventional keyhole reconstructed image (*k* = 170 lines) and (d) dynamic keyhole reconstructed image (*k* = 196 lines).

The zero-filling method in Figure 3(b) reused 152 lines with zeros, the conventional keyhole method in Figure 3(c) reused 170 lines, and the dynamic keyhole method in Figure 3(d) reused 196 lines. Compared to the other two methods, the dynamic keyhole method reused more *k* lines to reconstruct the same image quality, indicating a faster image acquisition time.

The performance of the three methods regarding the improvement of image quality was also evaluated. To provide a comparison of the image quality, an example of reconstructed images with 204 of 256 lines for a library across all the methods is shown in Figure 4.

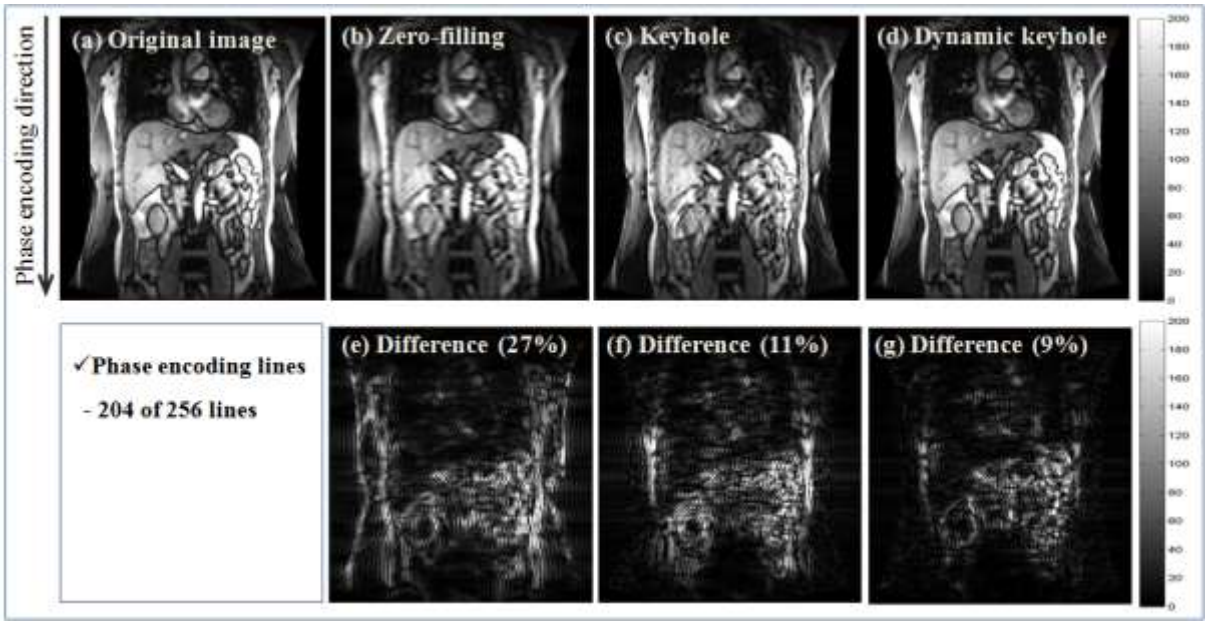

Figure 4. Reconstructed MR images utilizing (b) zero-filling, (c) conventional keyhole and (d) dynamic keyhole, where 204 of 256 lines were reused. (e), (f) and (g) display the difference between the original image (a) and the reconstructed images for the zero-filling (27%), conventional keyhole (11%), and dynamic keyhole (9%) methods, respectively.

From the reconstructed images shown in Figure 4, it is evident that the image quality of the dynamic keyhole method was superior to the zero-filling and conventional keyhole methods when 204 of 256 lines were reused. The reconstructed images using the zero-filling method in Figure 4(b) contained considerable blurring

image artifacts. The conventional keyhole image in Figure 4(c) produced better image quality than the zero-filling method, but still contained motion artifacts around regions affected by respiratory motion such as the diaphragm, kidneys, and liver. However, respiratory-related artifacts were minimized on the reconstructed image by the dynamic keyhole method in Figure 4(d).

The average number of *k* lines from the sixty datasets across the three methods using internal or external respiratory signals is shown in Table 1.

Table 1. Zero-filling, conventional keyhole and dynamic keyhole results of the mean and standard deviation (STD) of the number of *k* lines to achieve the same image quality difference compared with the original images for the sixty obtained datasets.

Methods	Mean ± STD of *k* lines
Zero-filling	162 (63%) ± 8
Conventional keyhole	188 (73%) ± 14
Dynamic keyhole (internal respiratory signal)	204 (79%) ± 17
Dynamic keyhole (external respiratory signal)	202 (78%) ± 17

Across the sixty datasets, the dynamic keyhole method using the internal respiratory signals reused an average of 204±17 of 256 (79%) lines compared to 162±8 of 256 (63%) lines in the zero-filling method and 188±14 of 256 (73%) lines in the conventional keyhole method to achieve the same difference from the ground truth image. The difference in the number of *k* lines between the dynamic keyhole method and the zero-filling or conventional keyhole method were statistically significant with a *p-value* < 0.0001 in both cases. There was a two-line difference in the average of *k* lines between the internal and external respiratory signals in the dynamic keyhole method (*p-value* < 0.0001). However, there was only a 1% difference, indicating that either internal or external respiratory signals are suitable for the dynamic keyhole method. The dynamic keyhole method required less scan time compared to the conventional keyhole method to achieve the same image quality during real-time central k-space dataset acquisition. For example, once the library of the prior peripheral k-space datasets were acquired, the real-time central k-space dataset acquisition of the dynamic keyhole method achieved image acquisition speeds of about 40 ms (52 of 256 lines) per image compared to about 53 ms (68 of 256 lines) per image for the conventional keyhole.

The performance of the dynamic keyhole method using the different input signals over the intra- and inter-subject variations is shown in Figure 5. For the intra- and inter-subject variations, sixty datasets were grouped by respiratory signal and subject.

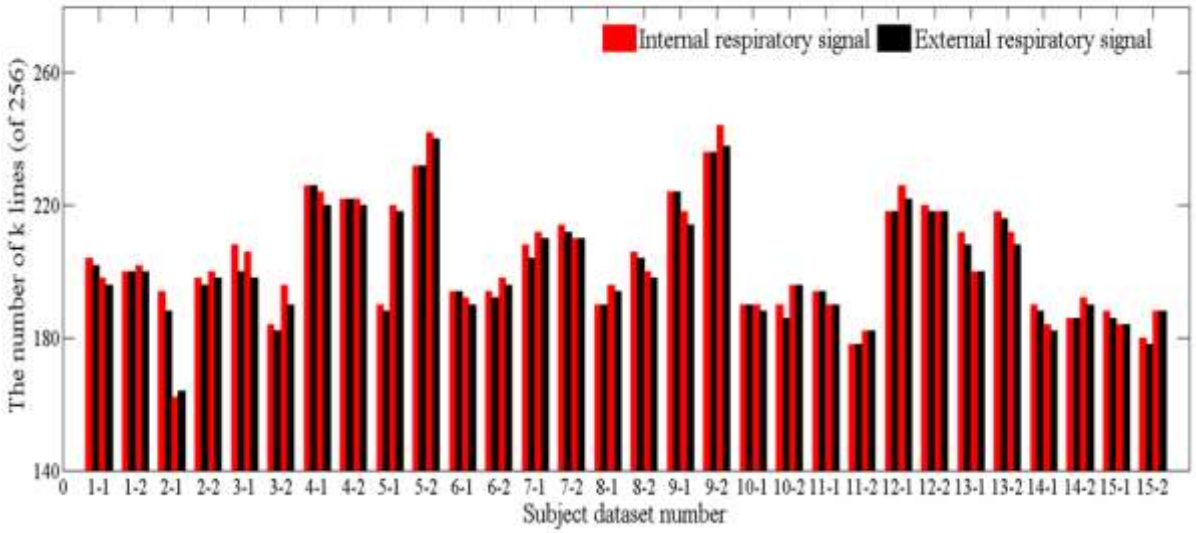

Figure 5. The number of *k* lines (of 256) for the dynamic keyhole method to achieve a 10% difference with the original image using the internal (red) and external (black) respiratory signals over the sixty obtained datasets of 15 subjects (two datasets, each with internal and external respiratory signals, over two imaging sessions). The subject dataset numbers are labeled by subject-imaging session, e.g. 5-2 is subject 5, session 2.

The internal respiratory signals compared to the external respiratory signal were similar in all of the sixty datasets. The largest difference was observed in subject 3, session 1, where eight more *k* lines were reused using the internal respiratory signals than the external signal. A larger difference in *k* lines was found when there were regular internal and relatively irregular external respiratory cycles, for example the datasets in subject 3, session 1 and subject 9, session 2. The *k* lines were lower with the internal respiratory signals in only one case, subject 2, session 1, due to irregular internal and relatively regular external respiratory signals.

The average of maximum-to-minimum range of intra-subject variation using internal (or external) respiratory signals and the standard deviation of *k* lines was 12±11 lines (or 12±10 lines). The average of maximum-to-minimum range of inter-subject variation across fifteen subjects and the standard deviation of *k* lines was 47±15 lines (or 49±16 lines).

IV. DISCUSSION

Real-time thoracic imaging often requires a large FOV and includes respiratory motion, leading to longer acquisition time and respiratory-related artifacts due to organ displacement. In this study, we introduced the dynamic keyhole method, which utilizes a library of prior peripheral k-space datasets corresponding to multiple respiratory states that are matched to real-time central k-space datasets using internal or external respiratory information. Using the dynamic keyhole method, we demonstrated fast image acquisition while maintaining image quality.

We demonstrated that the dynamic keyhole method resulted in a significant reduction in the amount of central k-space datasets necessary to acquire an image of sufficient quality. For the same amount of central k-space datasets, the dynamic keyhole method resulted in improved image quality compared to the zero-filling and conventional keyhole methods, as shown in Figures 3 and 4. The dynamic keyhole method reused 79% of prior peripheral k-space datasets to reconstruct artifact-free images, 6% more than conventional keyhole, and 16% more than zero-filling. As a result, the number of phase encoding lines was reduced by up to 79% from the full k-space acquisition during the central k-space dataset acquisition. This shows that the dynamic keyhole could be a valuable tool for fast MR image acquisition, which is required for real-time thoracic imaging in the presence of respiratory motion. In addition, the acquisition of full k-space datasets may not be necessary during library acquisition (Figure 1(A)(1)) when the same number of peripheral phase encoding lines is used. The scan time could be further reduced in this stage of the dynamic keyhole method if the k-space is not fully acquired.

To accelerate image acquisition time, compressed sensing[23, 24] and parallel imaging[32, 33] have been proposed for improving both acquisition time and quality of MR images. However, the delay between image acquisition and reconstruction in compressed sensing, due to the iterative reconstruction, and the sensitivity of multi-receiver coils in parallel imaging lead to residual aliasing and noise enhancement artifacts.[21] The barrier to real-time thoracic or abdominal imaging in compressed sensing could be, however, improved using the dynamic keyhole method. In compressed sensing, superior image quality of images reconstructed by the dynamic keyhole method could reduce iterations. Furthermore, the dynamic keyhole method can be combined with other undersampling methods, such as circular[18], radial[19], and spiral[20] to improve undersampling schemes for the out-of-field object size exceeding the diameter of FOV.[18]

In the current retrospective study, the internal respiratory signal measured directly from obtained images (manual process) was utilized.[30] This resulted in slightly better dynamic keyhole performance than the external respiratory signal in terms of *k*-line reduction. For prospective implementation, an automatically determined

diaphragm position[3, 25, 34] is necessary instead of the manual process utilized here, but it requires additional internal respiratory signal measurements whilst k-space datasets are measured and images reconstructed. Alternatively, the external respiratory signals can be easily utilized with only a small penalty in terms of *k*-line reduction, as there is a high internal-external signal correlation for the dataset used in this study (Pearson's R-value = 0.96).[31]

The dynamic keyhole method uses previously acquired full k-space datasets, and in an actual implementation, the library of k-space datasets for the prior peripheral k-space dataset and the central k-space dataset acquisition would be at a different frequency. Even though the library may be acquired at a lower temporal resolution, the dynamic keyhole method should give improved results over the conventional keyhole method because it utilizes multiple prior peripheral datasets matched to various respiratory displacements. In an additional study (data not shown), a temporal resolution of 800 ms was tested instead of 200 ms. In this case, the match between central and peripheral datasets was compromised; the library of a lower temporal resolution resulted in six fewer reused *k* lines on average compared with the 200 ms case. However, even in this case, the dynamic keyhole method was superior to the conventional keyhole when reusing an average of ten more *k* lines. Serially acquired peripheral dataset acquisitions corresponding to the same dataset magnitude as that needed for the real-time central k-space datasets could reduce data mismatch, but it would increase the time required to create the library.

The performance of the proposed dynamic keyhole method is reliant on the quality of the library and the ability to match it accurately to the central k-space datasets. After an additional simulation to find the optimum amount of datasets for the library, we suggest a greater number of breathing cycles when large cycle-to-cycle variations in respiratory displacement are present. This increase is to better account for variability in the subjects' breathing patterns. In an example from the subject 9, session 1, the number of *k* lines was measured at 186 and 200 lines when a single respiratory cycle and five respiratory cycles were used, respectively, due to irregular breathing (e.g. baseline drifts, overly deep/shallow breathing) during the library acquisition. The major factors leading to improved performance in the dynamic keyhole method were regular breathing[30] and the coverage of the library in respiratory displacements, which resulted in up to an 80% performance improvement with the internal respiratory signals and 70% with the external respiratory signals.

This study has demonstrated that the dynamic keyhole method is a promising MR image reconstruction technique applicable for real-time imaging of the thoracic and abdominal regions. The dynamic keyhole can be easily applied to a variety of pulse sequences and scanners, and can be combined with other fast imaging

techniques, such as k-space undersampling, and respiratory-gated imaging for real-time image guided radiotherapy, such as radiotherapy systems integrated with MRI.[7-9] A variety of inputs can be utilized for a respiratory signal, such as bellows belts[35], navigator[34], and ANZAI.[36]

V. CONCLUSION

In this study, the dynamic keyhole method utilized respiratory signals to improve MR images in the presence of respiratory motion, leading to a 79% reduction in central k-space datasets required for real-time MR imaging, while maintaining sufficient image quality. In addition, this was the first study in which MR image reconstruction utilized respiratory signals for real-time thoracic imaging. Our results suggest that the dynamic keyhole method could be a desirable technique for image-guided radiation therapy and MRI-guided radiotherapy that requires real-time MR monitoring in the thoracic region.

ACKNOWLEDGEMENTS

This project was supported by an NHMRC Australia Fellowship, NHMRC Program Grant APP1036078, and ARC Discovery Grant DP120100821. The authors thank Julie Baz and Robyn Keall for reviewing this paper for clarity.

REFERENCES

1 P.J. Keall, G.S. Mageras, J.M. Balter, R.S. Emery, K.M. Forster, S.B. Jiang, J.M. Kapatoes, D.A. Low, M.J. Murphy, B.R. Murray, "The management of respiratory motion in radiation oncology report of AAPM Task Group 76," Med. Phys. **33**, 3874 (2006).

2 L.I. Cervino, J. Du, S.B. Jiang, "MRI-guided tumor tracking in lung cancer radiotherapy," Phys. Med. Biol. **56**, 3773 (2011).

3 H.-X. Xu, M.-D. Lu, L.-N. Liu, L.-H. Guo, "Magnetic navigation in ultrasound-guided interventional radiology procedures," Clin. Radiol. **67**, 447-454 (2012).

4 I. Seimenis, N.V. Tsekos, C. Keroglou, E. Eracleous, C. Pitris, E.G. Christoforou, "An approach for preoperative planning and performance of MR-guided interventions demonstrated with a manual manipulator in a 1.5 T MRI scanner," Cardiovascular and interventional radiology **35**, 359-367 (2012).

5 K. Chida, Y. Kaga, Y. Haga, N. Kataoka, E. Kumasaka, T. Meguro, M. Zuguchi, "Occupational Dose in Interventional Radiology Procedures," American Journal of Roentgenology **200**, 138-141 (2013).

6 S. Kolling, B. Oborn, P. Keall, "Impact of the MLC on the MRI field distortion of a prototype MRI-linac," Med. Phys. **40**, 121705 (2013).

7 J.F. Dempsey, "System and method for image guidance during medical procedures," (WO Patent App. PCT/US2011/066,605, 2011).

8 B. Raaymakers, J. Lagendijk, J. Overweg, J. Kok, A. Raaijmakers, E. Kerkhof, R. van der Put, I. Meijsing, S. Crijns, F. Benedosso, "Integrating a 1.5 T MRI scanner with a 6 MV accelerator: proof of concept," Phys. Med. Biol. **54**, N229 (2009).

9 B. Fallone, B. Murray, S. Rathee, T. Stanescu, S. Steciw, S. Vidakovic, E. Blosser, D. Tymofichuk, "First MR images obtained during megavoltage photon irradiation from a prototype integrated linac-MR system," Med. Phys. **36**, 2084 (2009).

10 M. Uecker, S. Zhang, D. Voit, A. Karaus, K.D. Merboldt, J. Frahm, "Real-time MRI at a resolution of 20 ms," NMR in Biomedicine **23**, 986-994 (2010).

11 S. Zhang, A. Olthoff, J. Frahm, "Real-time magnetic resonance imaging of normal swallowing," JMRI2012).

12 A. Niebergall, S. Zhang, E. Kunay, G. Keydana, M. Job, M. Uecker, J. Frahm, "Real-time MRI of speaking at a resolution of 33 ms: Undersampled radial FLASH with nonlinear inverse reconstruction," Magn. Reson. Med2012).

13 M.L. Wood, R.M. Henkelman, "MR image artifacts from periodic motion," Med. Phys. **12**, 143 (1985).

14 J.J. Van Vaals, M.E. Brummer, W. Thomas Dixon, H.H. Tuithof, H. Engels, R.C. Nelson, B.M. Gerety, J.L. Chezmar, J.A. Den Boer, "“Keyhole” method for accelerating imaging of contrast agent uptake," JMRI **3**, 671-675 (1993).

15 R.K. Yang, C.G. Roth, R.J. Ward, D.G. Mitchell, "Optimizing Abdominal MR Imaging: Approaches to Common Problems1," Radiographics **30**, 185-199 (2010).

16 J.L. Duerk, J.S. Lewin, D.H. Wu, "Application of keyhole imaging to interventional MRI: a simulation study to predict sequence requirements," JMRI **6**, 918-924 (1996).

17 J.M. Hanson, Z.P. Liang, E.C. Wiener, P.C. Lauterbur, "Fast dynamic imaging using two reference images," Magn. Reson. Med **36**, 172-175 (1996).

18 K. Scheffler, J. Hennig, "Reduced circular field-of-view imaging," Magn. Reson. Med **40**, 474-480 (1998).

19 G. Glover, J. Pauly, "Projection reconstruction techniques for reduction of motion effects in MRI," Magn. Reson. Med **28**, 275-289 (2005).

20 C.H. Meyer, B.S. Hu, D.G. Nishimura, A. Macovski, "Fast spiral coronary artery imaging," Magn. Reson. Med **28**, 202-213 (2005).

21 K.T. Block, M. Uecker, J. Frahm, "Undersampled radial MRI with multiple coils. Iterative image reconstruction using a total variation constraint," Magn. Reson. Med **57**, 1086-1098 (2007).

22 D.C. Peters, P. Rohatgi, R.M. Botnar, S.B. Yeon, K.V. Kissinger, W.J. Manning, "Characterizing radial undersampling artifacts for cardiac applications," Magn. Reson. Med **55**, 396-403 (2006).

23 D.S. Smith, J.C. Gore, T.E. Yankeelov, E.B. Welch, "Real-Time Compressive Sensing MRI Reconstruction Using GPU Computing and Split Bregman Methods," International Journal of Biomedical Imaging **2012**2012).

24 R.G. Baraniuk, "Compressive sensing [lecture notes]," Signal Processing Magazine, IEEE **24**, 118-121 (2007).

25 R. Song, A. Tipirneni, P. Johnson, R.B. Loeffler, C.M. Hillenbrand, "Evaluation of respiratory liver and kidney movements for MRI navigator gating," JMRI **33**, 143-148 (2011).

26 O. Wade, "Movements of the thoracic cage and diaphragm in respiration," The Journal of physiology **124**, 193-212 (1954).

27 H.W. Korin, R.L. Ehman, S.J. Riederer, J.P. Felmlee, R.C. Grimm, "Respiratory kinematics of the upper abdominal organs: a quantitative study," Magn. Reson. Med **23**, 172-178 (1992).
28 S. Davies, A. Hill, R. Holmes, M. Halliwell, P. Jackson, "Ultrasound quantitation of respiratory organ motion in the upper abdomen," British journal of radiology **67**, 1096-1102 (1994).
29 A. Stemmer, B. Kiefer, "Phase navigator for respiratory triggering," Proceedings of the 18th Annual Meeting of ISMRM, Stockholm, Sweden (2010).
30 T. Kim, S. Pollock, D. Lee, R. O'Brien, P. Keall, "Audiovisual biofeedback improves diaphragm motion reproducibility in MRI," Med. Phys. **39**, 6921 (2012).
31 H. Steel, S. Pollock, D. Lee, P. Keall, T. Kim, "The internal–external respiratory motion correlation is unaffected by audiovisual biofeedback," Australasian Physical & Engineering Sciences in Medicine, 1-6 (2014).
32 J. Carlson, T. Minemura, "Imaging time reduction through multiple receiver coil data acquisition and image reconstruction," Magn. Reson. Med **29**, 681-687 (2005).
33 A. Deshmane, V. Gulani, M.A. Griswold, N. Seiberlich, "Parallel MR imaging," JMRI **36**, 55-72 (2012).
34 P. Spincemaille, T.D. Nguyen, M.R. Prince, Y. Wang, "Kalman filtering for real-time navigator processing," Magn. Reson. Med **60**, 158-168 (2008).
35 C. Santelli, R. Nezafat, B. Goddu, W.J. Manning, J. Smink, S. Kozerke, D.C. Peters, "Respiratory bellows revisited for motion compensation: Preliminary experience for cardiovascular MR," Magn. Reson. Med **65**, 1097-1102 (2011).
36 X.A. Li, C. Stepaniak, E. Gore, "Technical and dosimetric aspects of respiratory gating using a pressure-sensor motion monitoring system," Med. Phys. **33**, 145 (2006).

(A) Dynamic Keyhole

(B) Conventional Keyhole

Prior Peripheral Dataset (Library) Acquisition

(1) Acquire respiratory signals and full k-space datasets

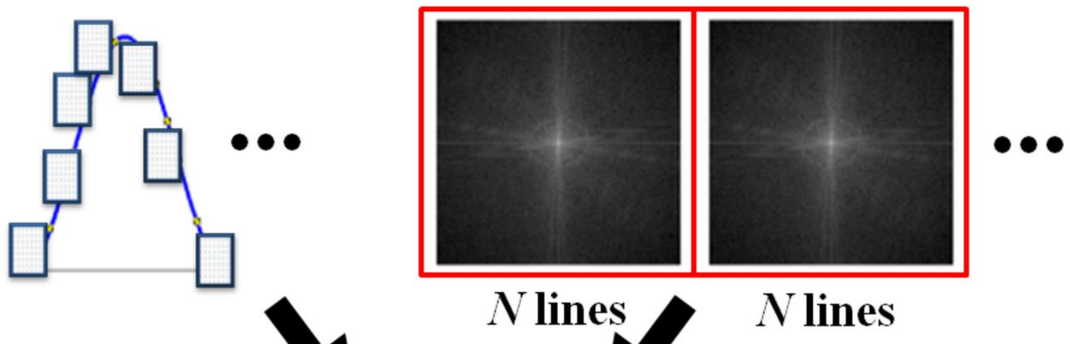

(2) Determine the number of *k* lines within tolerance (*T*)

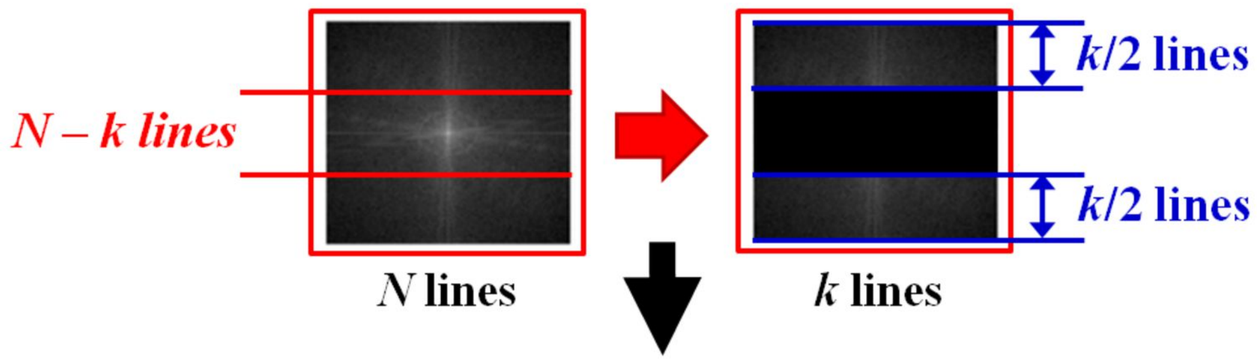

(3) Build the library of prior peripheral k-space datasets across respiratory displacements

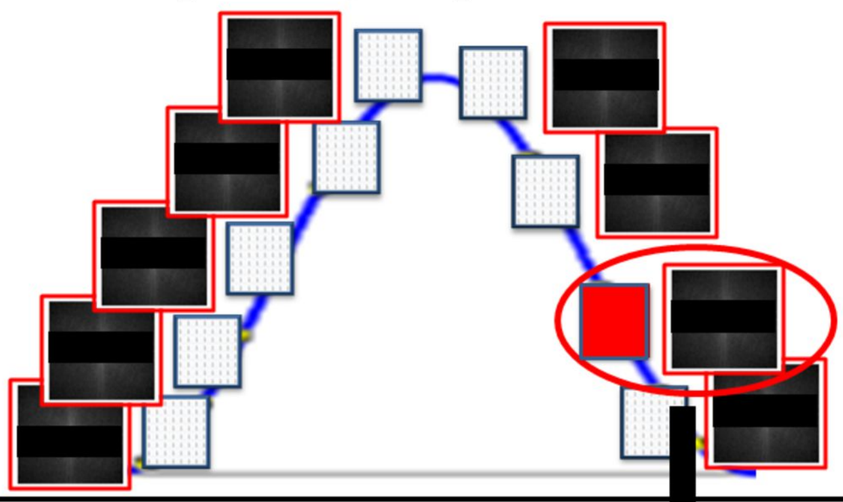

Real-time Central Dataset Acquisition

(4) Match respiratory displacement

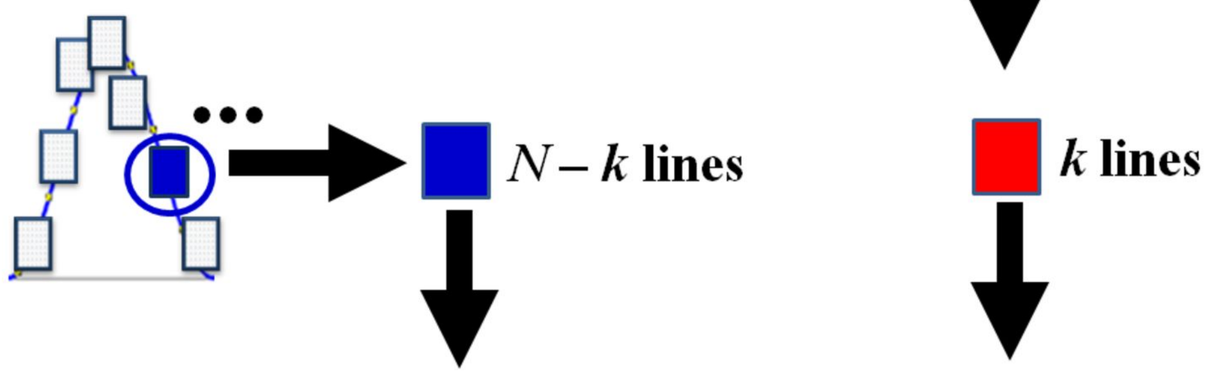

(5) Combine central k-space and prior peripheral k-space

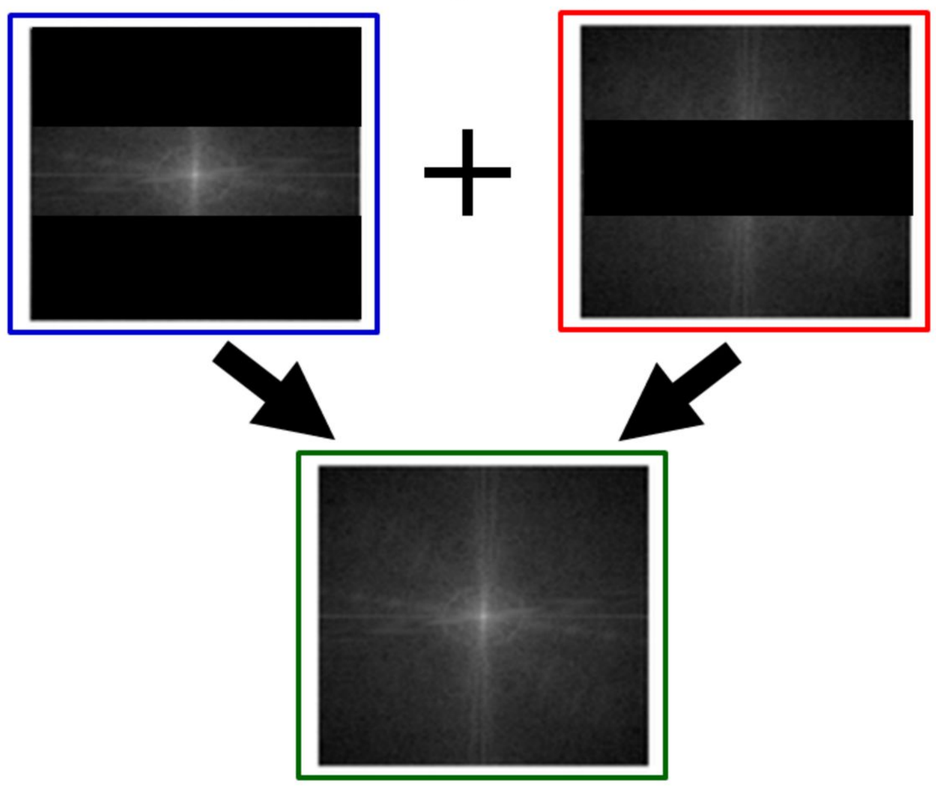

Acquire full k-space (*N*) lines

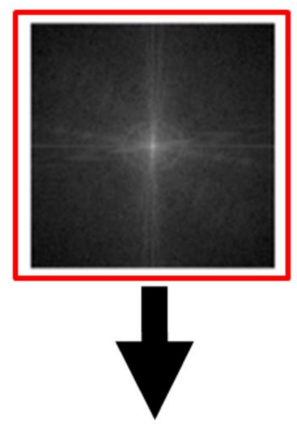

Determine a prior peripheral k-space dataset

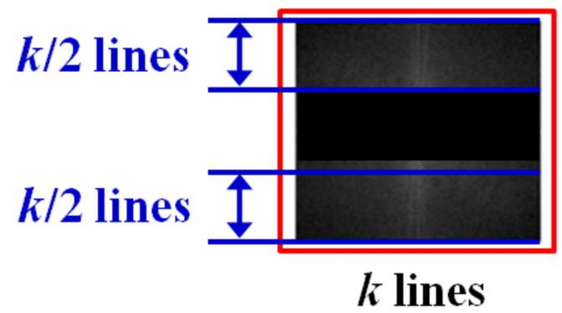

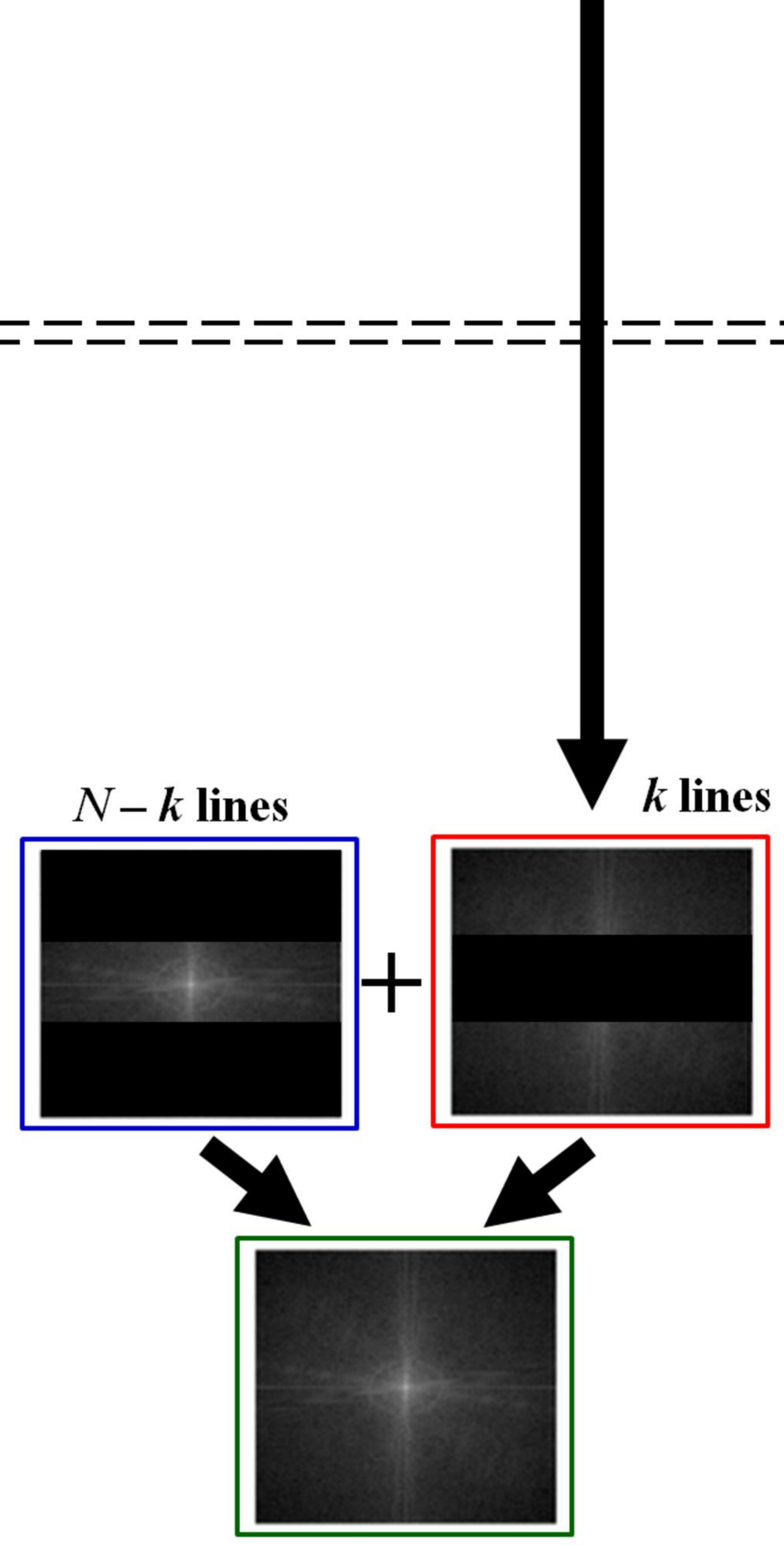

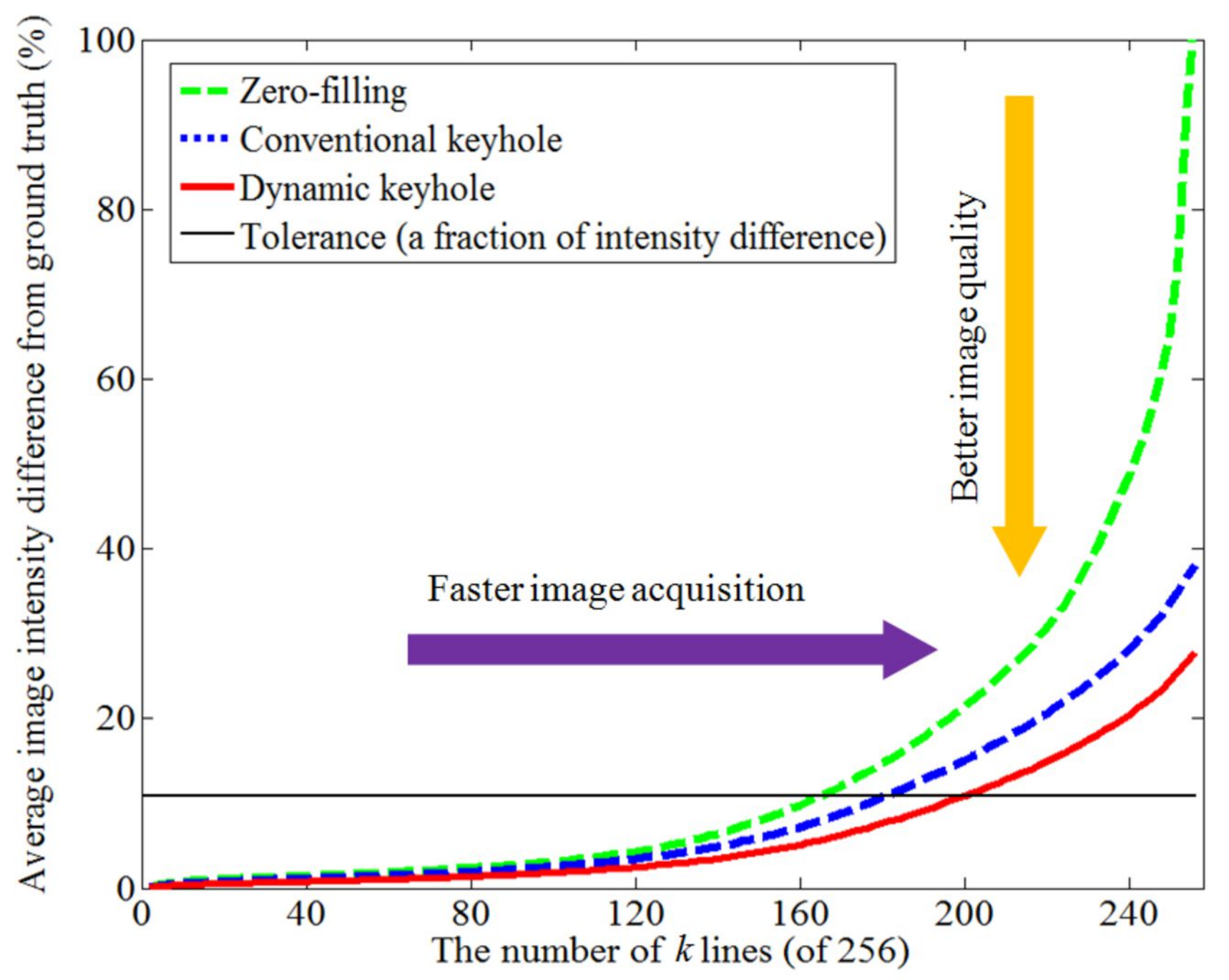
Zero-filling
Conventional keyhole
Dynamic keyhole
Tolerance (a fraction of intensity difference)
Better image quality
Faster image acquisition
Average image intensity difference from ground truth (%)
The number of k lines (of 256)
0
20
40
60
80
100
0
40
80
120
160
200
240

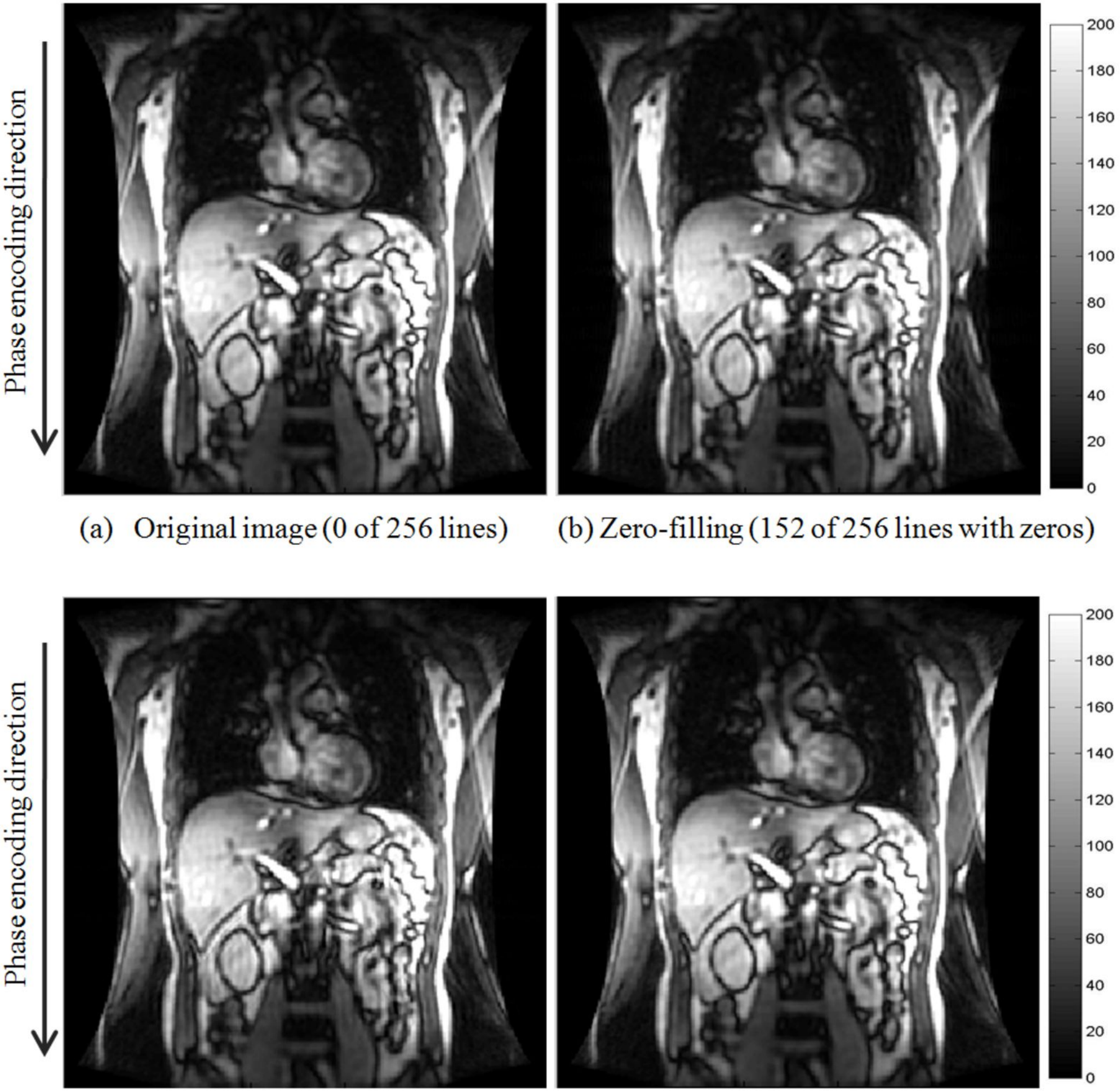

(a) Original image (0 of 256 lines)

(b) Zero-filling (152 of 256 lines with zeros)

(c) Conventional keyhole (170 of 256 lines)

(d) Dynamic keyhole (196 of 256 lines)

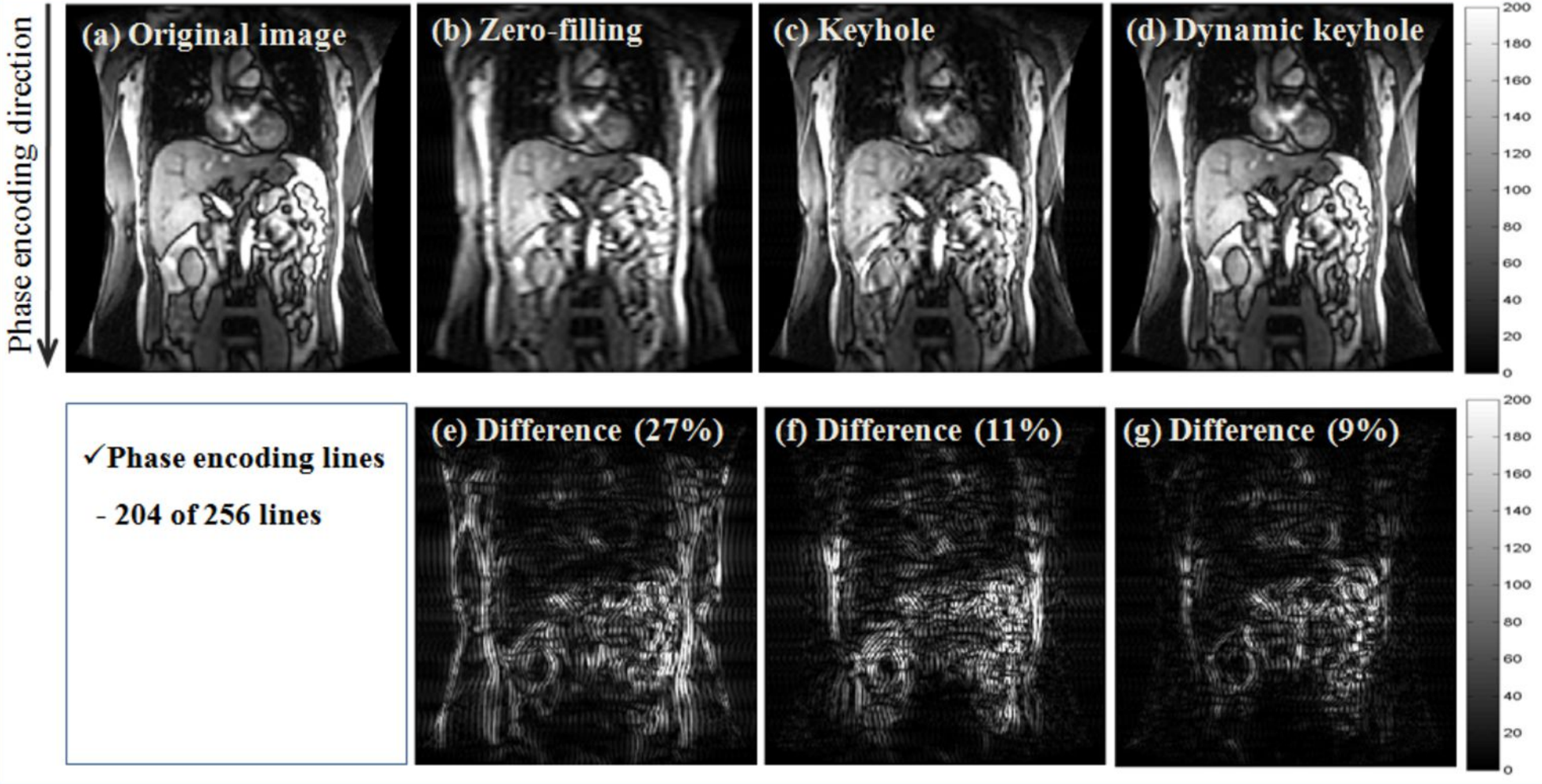
Phase encoding direction
(a) Original image
(b) Zero-filling
(c) Keyhole
(d) Dynamic keyhole
200
180
160
140
120
100
80
60
40
20
0
✓Phase encoding lines
- 204 of 256 lines
(e) Difference (27%)
(f) Difference (11%)
(g) Difference (9%)
200
180
160
140
120
100
80
60
40
20
0

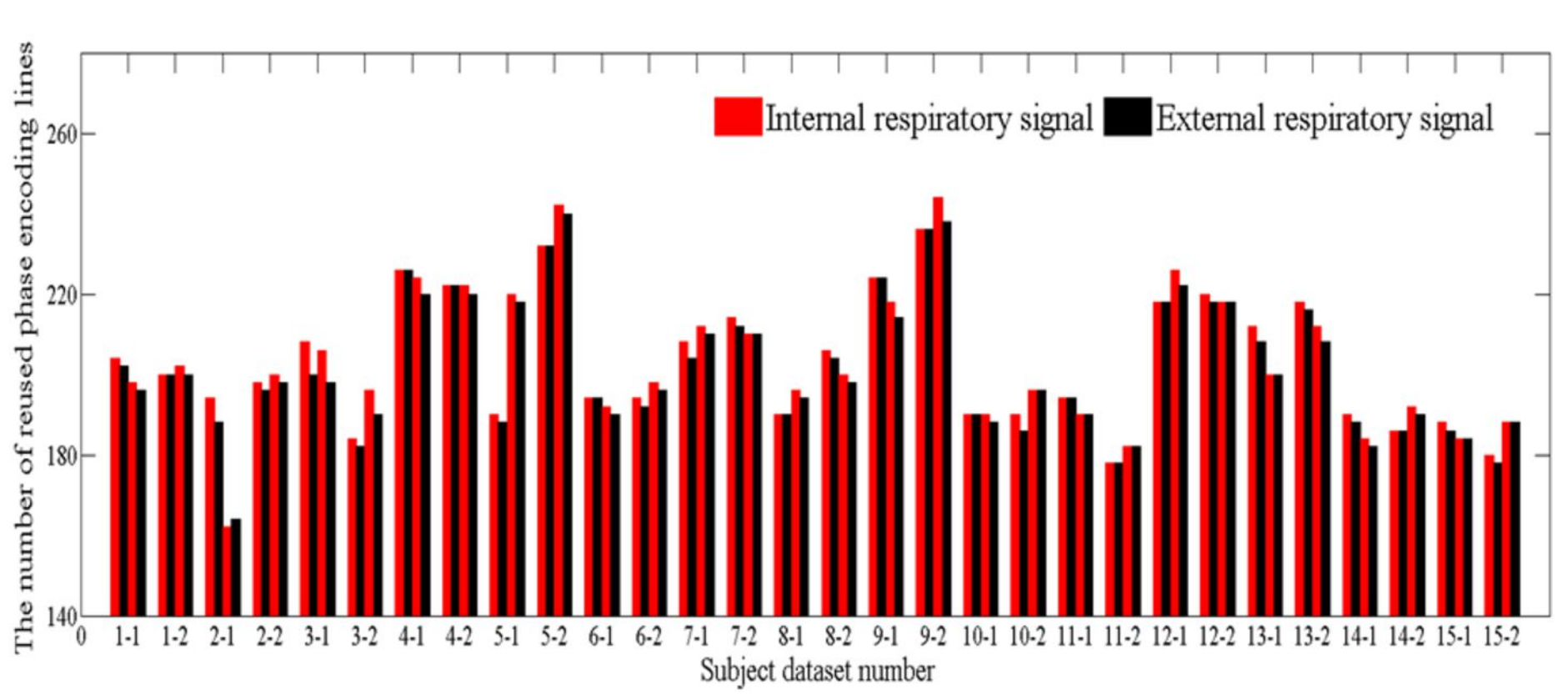
Internal respiratory signal
External respiratory signal
The number of reused phase encoding lines
140
180
220
260
0
1-1
1-2
2-1
2-2
3-1
3-2
4-1
4-2
5-1
5-2
6-1
6-2
7-1
7-2
8-1
8-2
9-1
9-2
10-1
10-2
11-1
11-2
12-1
12-2
13-1
13-2
14-1
14-2
15-1
15-2
Subject dataset number